Version of Record: https://www.sciencedirect.com/science/article/pii/S0142112320306095
Manuscript_e9865ea2d03743c898339b14704fcc95

Slip Delocalization and Diffusion Mediated Carbide Formation during Fatigue of a Nickel-Base Superalloy

Yejun Gu[b], Jean Charles Stinville[a,*], Patrick G. Callahan[c], McLean P. Echlin[a], Tresa M. Pollock[a], Jaafar A. El-Awady[b]

[a] *Materials Department, University of California Santa Barbara, Santa Barbara, California 93106-5050*
[b] *Department of Mechanical Engineering, Whiting School of Engineering, The Johns Hopkins University, Baltimore, Maryland, 21218*
[c] *US Naval Research Lab, Washington, DC, USA*

Abstract

Fatigue crack initiation at high temperatures occurs at microscopic fatigue shear bands that form near twin boundaries in polycrystalline nickel-base superalloys that contain minimal metallurgical defects. The associated dislocation sub-structure is complex and dependent on thermal and mechanical conditions. Here we show the formation of fine-scale carbide precipitates along these fatigue shear bands in a nickel-base superalloy during fatigue above 650°C. The formation of carbide precipitates is studied using calculations of bulk and pipe diffusion. The contribution of pipe diffusion is observed to be critical in the formation of fine-scale carbides and occurs coincident with the delocalization of slip during fatigue.

Keywords: René 88DT Polycrystalline Nickel-Base Superalloy, Coherent Twin Boundary, Carbide Precipitation, Bulk and Pipe Diffusion, Microscopic Fatigue Shear Band, Persistent slip band

1. Introduction

Polycrystalline nickel-base superalloys possess exceptional monotonic mechanical properties at high temperatures that make them suitable for use in hot sections of gas turbine engines. However, fatigue of polycrystalline nickel-base superalloys used for turbine disks is a limiting property [1]. Their fatigue strengths can be as low as 40% of their yield strengths [2]. Alloys processed through advanced powder metallurgy have low concentrations of pores, inclusions, and other extrinsic defects, which can act as fatigue crack initiation sites. As a consequence, competing failure modes occur between the grain-structure or non-metallic inclusions [3]. Moreover, fatigue cracks often initiate on surfaces with relatively low roughness at intrinsic microstructural configurations [4, 5, 6, 7, 8, 9, 3, 10]. Thus, identifying and characterizing the local microstructure configurations that are amenable to the initiation of

*corresponding author
Email address: stinville@engr.ucsb.edu (Jean Charles Stinville)

cracks is crucial for improving fatigue life performances and design of new generations of polycrystalline nickel-base superalloys.

Numerous studies [4, 5, 6, 7, 8, 9, 3] on the low, high, and very high cycle fatigue behavior of polycrystalline nickel-base superalloys indicate that cyclic strain localization occurs on {111} planes near and parallel to specific Σ3 twin boundaries in grains oriented for parallel slip [3]. It is for this local microstructure configuration that fatigue cracks initiate at and above room temperature. The formation of microscopic fatigue shear bands have been observed for these microstructure configurations by transmission electron microscopy (TEM) in nickel-base superalloys cycled at high temperatures [3, 11, 12, 13]; this is in contrast to the conventional observations of deformation bands [13] or persistent slip bands with ladder-like structures [14] in single phase materials. These fatigue shear bands tend to develop in a very localized manner and with relatively disorganized structures containing dislocation debris within the primary glide planes, as described in detail for the nickel-base superalloy René 88DT during cyclic loading at room [15] and high temperatures [3]. The fatigue shear bands have been observed to thicken during cyclic loading by the activation of sequential {111} parallel slip planes [3], indicative of a delocalization phenomenon. In addition, a relatively high density of dislocations can develop between the primary planes where glide occurs. The dislocation mechanisms that operate at intermediate and high temperatures near twin boundaries, which allow for the dislocations to glide outside the primary {111} activated planes, are still not clearly identified. There are several mechanisms that can account for the formation of fatigue shear bands, such as hardening on the main plane where glide is occurring, including K-W locks [16], strain aging [17, 18, 19, 20, 21, 22], or fine-scale carbide precipitation [23]. These effects are in combination with the enhancement of thermally activated mechanisms like cross slip that manifest at high temperatures [24] and enable the movement of a dislocation from one plane to another, forming microscopic fatigue shear bands that are comprised of multiple parallel {111} slip bands.

During fatigue of nickel-base alloys at high temperature, microstructural changes such as γ' precipitate coarsening or carbide formation can occur, significantly modifying the dislocation structure associated with the fatigue shear bands. Of interest, the precipitation of fine-scale carbides on slip bands has previously been observed in nickel-base superalloy to be important in the fatigue crack nucleation during cyclic loading at high temperature [23, 25]. Extended formation of carbides during fatigue at high temperature leads to embrittlement of slip bands and favors oxidation processes, therefore reducing the fatigue life [23]. However, these processes are observed at temperatures higher than 700°C. Here, we show that nanometer-scale scale carbide precipitates occur at temperatures lower than 700°C and immobilize dislocations and enhance hardening on the main glide planes, which may also lead to the activation of new mobile dislocations on subsequent parallel planes to carry the imposed deformation, contributing to an increase in fatigue life. While extended carbide formation during fatigue at temperatures higher than 700°C is detrimental, the formation of fine-scale carbide at temperature lower than 700°C may be beneficial. In the present study, the slip delocalization phenomenon associated with the increase in fatigue life with increasing testing temperature is detailed and the precipitation of fine-scale carbides during fatigue inside the microscopic fatigue shear bands for the nickel-base superalloy René 88DT

is characterized. In addition, a proposed mechanism for the precipitation of carbides during fatigue is investigated by considering the bulk and pipe diffusion of carbon. A discussion of the results is then presented, followed by a summary and conclusion.

2. Experimental procedure

2.1. Material

Cylindrical polycrystalline powder metallurgy processed René 88DT specimens with a gauge diameter of 10 mm and gauge length of 45 mm were used in this study. The nominal composition of René 88DT is 13%Co, 16%Cr, 4%Mo, 4%W, 2.1%Al, 3.7%Ti, 0.7%Nb, 0.04%C, 0.015%B (wt%) [26]. The microstructure of the alloy consists of a γ matrix with a face-centered cubic (FCC) crystal structure and γ' precipitates having a $L1_2$ crystal structure. As heat treated, there are larger secondary precipitates with sizes on the order of 100-200 nm and smaller tertiary γ' precipitates with sizes on the order of several nm within the γ grains [26]. The Cr, which participates in the formation of the carbides, strongly partitions to the matrix [7]. The grain sizes and orientations of the alloy were previously characterized using electron back scatter diffraction (EBSD) [4], which showed that the material exhibits little crystallographic texture, a large fraction of $\Sigma 3$ boundaries (58% of the total boundary length fraction), an average grain size of 26 um, and a small number of large grains that are two to five times larger than the average grain size. Monotonic testing revealed a 0.2% offset yield strengths of 1180 MPa (at ≈0.75% total stain) and 985 MPa (at ≈0.7% total stain) at room temperature and 593°C, respectively [27].

2.2. Mechanical tests

Cyclic testing was performed on an electromechanical machine in a symmetric, uniaxial, push-pull mode in vacuum at 400 °C and 650 °C in the high cycle fatigue (HCF) regimes at an imposed strain of about 0.4% (nominal elastic regime). High temperature tests were carried out in strain control mode with R-ratios near zero and at a frequency of 0.5 Hz. Heating was performed using a resistive furnace with temperature in the gauge section controlled to ± 7 °C. Typical fatigue life between 100,000 to 300,000 cycles is observed resulting in fatigue test duration between 13 to 40 hours. Room temperature fatigue data of the same alloys, previously published in [6], are used as comparison. Room temperature tests were carried out in stress control mode at a frequency of 1 Hz with an equivalent strain of about 0.4% (nominally elastic regime). Typical fatigue life below 100,000 is observed.

2.3. Characterization techniques

Conventional scanning transmission electron microscopy (STEM) and high resolution transmission electron microscopy (HRTEM) were performed in an FEI Titan at 300 kV. Conventional transmission electron microscopy (TEM) was performed using an FEI Tecnai operated at 200 kV. The TEM foils were extracted from specific areas post deformation using the standard focused ion beam (FIB) cross sectioning and lift-out technique inside a FEI Helios dual beam FIB-SEM. The foils were incrementally thinned to approximately 100 nm using decreasing voltage and current from 16 kV and 45 pA to 2 kV and 10 pA to minimize

FIB damage. A total of more than 15 foils were extracted from different specimens at regions of interest across the temperature regimes.

3. Experimental observations

Fatigue specimens tested at room temperature, 400°C and 650°C in the HCF regime display the formation of microscopic fatigue shear bands near specific twin boundaries during cyclic loading as shown in Figure 1. These fatigue shear bands are observed to be at the origin of surface crack initiation at room temperature and internal crack initiation at 650°C [9, 3]. However, the structure of the fatigue shear band at room and high temperature is significantly different. The shear bands formed during cyclic loading at 650°C at 80% of the fatigue life, shown in Figure 1(c-f), have multiple parallel slip bands parallel and offset from the twin boundaries, and contain a high density of dislocations between the bands as shown in Figure 3(a). Further details of this experiment are given elsewhere [3]. Surface extrusions are also observed along the primary {111} slip system as shown in Figure 1(c-f). The FIB cross-sectioned profile of the intrusions/extrusions that are aligned with one of these microscopic shear bands is shown in Figure 1(f). While the slip activity extends over a large area near twin boundaries at 650°C, the activity at room temperature is restricted to the vicinity of the twin boundary as shown in Figure 1(a-b). The extrusion of material at the surface is significant at room temperature (Figure 1(b)) and reduced at 650°C ((Figure 1(c-e)).

The average thicknesses of fatigue shear bands at the surface of the specimen for specimens tested at room temperature, 400°C and 650°C are displayed in Figure 2(a) as a function of the normalized fatigue life. The thickness of fatigue shear band is defined as the distance between the twin boundary and the farthest slip trace that constitutes the fatigue shear band, as depicted by the red arrow in Figure 1(e). 50 fatigue shear bands were investigated in different specimens for the three test temperatures. It is observed that the thickness of the fatigue shear bands increases with increasing temperature and number of cycles. The surface crack density at 80% of fatigue life is displayed in Figure 2(b) for specimens tested at room temperature, 400°C and 650°C. While the thickness of the fatigue shear bands increases with temperature, the surface crack density decreases with temperature. No surface cracks were observed for specimens tested in the high cycle fatigue regime at 650°C.

Interestingly, fine-scale precipitates in the γ matrix that developed along the primary slip bands during cyclic loading at 650 °C are observed in Figure 3 in a foil extracted perpendicular to the shear band. However, these fine-scale precipitates are not observed in specimens tested at 450°C and room temperature. The diffraction patterns of the volume inside the red dashed circle around the fine-scale precipitates (Figure 3(d)) are shown in Figure 3(e) and (f) for the (112) and (011) zone axis, respectively. The patterns correspond to the $M_{23}C_6$ phase as confirmed by the simulated patterns in the inserts of Figure 3(e) and (f). The extra reflections result from diffraction from the γ and γ' phases in the volume. The $M_{23}C_6$ phase has a cube on cube orientation relationship with the γ phase [28]. High resolution TEM at the location of a carbide precipitate is shown in Figure 4(a). The theoretical stress-free atomistic arrangement for the Ni_3Al and $M_{23}C_6$ phases was simulated and

shown in Figure 4(b) and (c), respectively. In addition, the chemical composition measured by energy dispersive X-ray analysis (EDS) HRTEM along a line scan across the carbide precipitate in Figure 4(d) shows that a significant amount of chromium is in the carbide precipitate, which suggests that the fine-scale precipitation is associated with the formation of $Cr_{23}C_6$ in the matrix.

The effect of the formation of these carbides on the structure of the fatigue shear band is discussed later. First, the origin of the carbides using a diffusion model is discussed. The carbide formation can be divided into a nucleation stage and a coarsening stage. Carbides most likely nucleate at jogs/kinks, dislocation junctions [29], and/or at the intersection of a dislocation with a grain boundary or precipitate interface [29]. These sites act as pinning points for dislocations and trapping sites for C atoms. For a carbide to nucleate at a dislocation, the concentration of C atoms at the dislocation must first reach supersaturation. This supersaturation zone serves as the nucleus of the carbide and also leads to dislocation pinning. Supersaturation around the dislocation core is predominantly controlled by bulk diffusion of C atoms driven by the stress field of the dislocation.

4. Diffusion Model for the Carbide Formation

The carbide formation requires the diffusion of both C and Cr atoms to the location of the carbide while all other atoms (e.g. Ni, Co etc.) hldiffusing away from the carbide. Thus, diffusion analysis are conducted here to show that the formation of a carbide nuclei during fatigue at high temperatures is assisted by bulk diffusion of C atoms, while its growth is predominantly attributed to pipe diffusion. The time required for the formation of a carbide nuclei and its coarsening will also be estimated. To start with, it is assumed that the critical time for the carbide formation is determined by the diffusion of C atoms. This assumption is then validated at the end of this section.

From the TEM observation, the average spacing between the carbides is around 150 nm along the Burgers vector direction and approximately 200 nm along the edge direction, and the spacing between neighboring slip planes is $\approx$ 150 nm. The average size of observed carbides is around 16.5$\times$ 36.4$\times$100 nm^3. Therefore, the average volume of a carbide precipitate is $V_{carbide}$=6.0 $\times$ 10^4 nm^3. The previous information and a typical duration of $t = 6.84 \times 10^4$ s for a fatigue test is used in the following calculation.

As a first order approximation, it is assumed that René 88DT can be constructed from repeated unit cells of the same atomic concentrations in the matrix and in the carbide, respectively. The number and type of the different atoms in each unit cell are determined based on the composition of the the γ matrix and the carbide. A matrix unit cell containing one C atom is referred to as the "matrix cell". The different elements in the γ matrix, their atomic masses, and the number of atoms of each element in the matrix cell are summarized in Table 1. Because the numbers of Zr and B atoms in the matrix are far less than the number of C atoms, they are ignored here for simplicity. The reference C atom fraction in the alloy matrix is defined as the ratio between the number of C atoms and the total number

of substituional atoms in the matrix cell:

$$X_0 = \frac{1}{N_{\text{MatrixCell}}} = 0.00318, \tag{1}$$

where $N_{\text{MatrixCell}}$ is the total number of substituional atoms in a matrix cell.

Table 1: Composition of the René 88DT γ matrix, atomic mass and volume of each element, as well as the number of atoms of each element in a matrix cell.

Element	Cr	Co	Mo	W	Ti	Al	Nb	Zr	C	B	Ni
wt% in the γ matrix	22	17	6	3.3	0.7	0.7	0.3	-	0.06	-	43.64
Atomic mass (u)	52	59	96	184	48	27	93	91	12	11	59
Number of atoms in the matrix cell	84.5	57.5	12.5	3.5	3	5	0.5	0	1	0	148

Given that the matrix has an FCC structure and the lattice parameter is 0.3589 nm, an average Bravais FCC unit cell containing 4 Ni or substituional atoms is $V_{\text{FCC}} = 0.046\,23\,\text{nm}^3$. Since a matrix cell contains 314.5 Ni and substitutional atoms, the volume of the matrix cell is $V_{\text{MatrixCell}} = V_{\text{FCC}}/4 \times 314.5 = 3.64\,\text{nm}^3$. On the other hand, the unit cell of a carbide precipitate is composed of 23 Cr and 6 C atoms, which occupies a volume, $V_{\text{Cr}_{23}\text{C}_6} = 0.294\,\text{nm}^3$ [30].

4.1. Supersaturation Time Analysis

The bulk diffusion of C atoms can be described by the following diffusion equation [31, 32]:

$$\frac{\partial X}{\partial t} = D_b \bigtriangledown \cdot \left[\bigtriangledown X + \frac{X \bigtriangledown V}{k_{\text{B}} T} \bigtriangledown P \right], \tag{2}$$

where X is the C atom fraction in the alloy matrix, D_b is the bulk diffusion coefficient of C in the matrix, $P = -\sigma_{kk}/3$ is the hydrostatic pressure, $\Delta V = 1.73 \times 10^{-30}\,\text{m}^3$ is the volume change associated with the insertion of a C atom in the matrix [33], k_{B} is the Boltzmann constant, and T is the temperature. In the presence of a defect the hydrostatic pressure in Eq. (2) should be computed from the stress field induced by that defect.

The C bulk diffusion was computed for pure Ni as a function of temperature [34], $D_b = 2.5 \times 10^{-4} \times \exp\left(-20200/T\right)\,\text{m}^2\,\text{s}^{-1}$, where T is in unit of K. For reference, D_b is equal to $2 \times 10^{-11}\,\text{m}^2\,\text{s}^{-1}$ at a temperature 957 °C [34]. These values are used in the current analysis since to our knowledge there are no data reported for C bulk diffusion in any nickel-base superalloy.

The fraction of C atom at saturation around a defect is thus (i.e. when $\frac{\partial X}{\partial t} = 0$):

$$X_C^{Sat} = X_0 \exp\left(-\frac{P \bigtriangledown V}{k_{\text{B}} T}\right). \tag{3}$$

In the current experiments most carbides are observed along a shear band, thus the formation of carbides are assumed to initiate in the vicinity of a dislocation (edge or screw). For a cylindrical volume surrounding a straight dislocation segment of length l_d and having cross-sectional area A_d perpendicular to the dislocation line, the reference number of C atoms can now be computed from the integral:

$$N_{\mathrm{C}}^{\prime\,0} = N_{\mathrm{MatrixCell}} \int_{A_d} X \frac{l_d \mathrm{d}s}{V_{\mathrm{MatrixCell}}}, \tag{4}$$

where ds is an infinitesimal area element. At saturation, the number of C atoms in the same cylindrical region can then be computed from Eqs. (3) and (4):

$$N_{\mathrm{C}}^{\prime\,Sat} = N_{\mathrm{MatrixCell}} \int_{A_d} X_0 \exp\left(-\frac{P \bigtriangledown V}{k_{\mathrm{B}} T}\right) \frac{l_d \mathrm{d}s}{V_{\mathrm{MatrixCell}}}. \tag{5}$$

The interaction energy and the concentration of C atoms decreases significantly with increasing distance from the dislocation core [35], so in the current analysis the characteristic length of A_d was defined as 7.6 nm (i.e. $30b$), and the bulk diffusion of C atoms described by Eq.(4) is solved in a square domain having an edge length of 330 nm. In addition, based on the observed carbide spacing, the dislocation length involved is assumed to be $l_d \approx 100$ nm. All the calculations are performed for the case of an edge dislocation, which is expected to have a stronger effect than screw dislocations [35].

The percentage of C atoms relative to the saturation limit as a function of time for three different temperatures: 200 °C, 500 °C and 700 °C, are shown in Figure 5. It is clear that with increasing temperature the time needed to reach supersaturation around an edge dislocation decreases dramatically. At 200 °C it takes more than 1000h to reach 99.8% of C saturation around an edge dislocation, while at 700 °C it takes less than 1 microsecond. In these analyses it is assumed that the dislocation is stationary for the entire duration of the C diffusion process. These analyses therefore suggest that carbide nucleation is more likely to take place at temperatures ≥ 500 °C, while below this temperature it is highly unlikely.

4.2. Coarsening Time Analysis

The secondary γ' is considered as C-poor with respect to the matrix [36]. Therefore, given the size of the matrix cell and the volume ratio between the γ matrix and secondary γ'(i.e. 1 : 0.66 [26]), the average distance between C atoms in the alloy is:

$$l_{\mathrm{C-C}} = \left(\frac{V_{\mathrm{MatrixCell}}}{1.0} \times 1.66\right)^{1/3} = 1.82\,\mathrm{nm}. \tag{6}$$

Considering the average volume of a carbide precipitate, V_{Carbide}, based on TEM observations, the number of C atoms required to build a single carbide is:

$$N_{\mathrm{C}}^{f} = \frac{V_{\mathrm{Carbide}}}{V_{\mathrm{Cr_{23}C_6}}} \times 6 = 1.22 \times 10^6 \quad \text{atoms} \tag{7}$$

Additionally, the number of C atoms that are already present in the volume in which a carbide will form can be estimated as:

$$N_{\mathrm{C}}^{0} = \frac{V_{\mathrm{Carbide}}}{V_{\mathrm{MatrixCell}}} \times 1 = 1.65 \times 10^{4} \quad \text{atoms} \tag{8}$$

Therefore, the number of additional C atoms that needs to be transported from the matrix to the location of the carbide is $N_{\mathrm{C}}^{t} = N_{\mathrm{C}}^{f} - N_{\mathrm{C}}^{0} \approx 1.2 \times 10^{6}$ atoms.

Assuming that only one single C atom can pass through the dislocation core at any time, the distance of the furthest C atom to be transported to the carbide is:

$$L = \frac{N_{\mathrm{C}}^{t} l_{\mathrm{C-C}}}{n}. \tag{9}$$

where n is the number of dislocations paths available to transport C atoms to the location of the carbide. Using the Einstein formula and ignoring the C concentration gradient, the average velocity of a C atom transported along the dislocation is [37]:

$$v = \frac{D_p \Delta V \nabla_{\boldsymbol{\xi}} P}{k_{\mathrm{B}} T} = \frac{L}{t}, \tag{10}$$

where $\nabla_{\boldsymbol{\xi}} P = 0.2\,\mathrm{GPa\,\mu m^{-1}}$ is the typical gradient of the hydrostatic pressure in the dislocation line direction, $\boldsymbol{\xi}$ [38, 39].

It should be noted that the C pipe diffusion coefficient is a function of temperature. However, to our knowledge there is no available estimate for C pipe diffusion in pure Ni or in nickel-base superalloys. Furthermore, pipe diffusion is typically higher than bulk diffusion at low temperature but at higher temperatures their values are comparable. For example, it was shown in alpha-iron that the C bulk diffusion coefficient is close to the C pipe diffusion coefficient around 700 °C [40]. Therefore, in the current analysis a simplified relation between the C bulk diffusion coefficient and C pipe diffusion coefficient is assumed based on those reported for C in alpha-iron [40] and Si in Al [37] as an approximation of the C pipe diffusion coefficient in nickel-base superalloys:

$$D_p = D_b \times 10^{4-3T/1000}, \tag{11}$$

where T is in unit of K. As indicated by Eq. (11), pipe diffusion is predominant at temperatures below 1060 °C. However, for higher temperatures bulk diffusion is more dominant. From Eqs. (9) and (10) the number of dislocation paths needed is:

$$n = \frac{N_{\mathrm{C}}^{t} l_{\mathrm{C-C}} k_{\mathrm{B}} T}{D_p \Delta V \nabla_{\boldsymbol{\xi}} P t}. \tag{12}$$

Based on the average spacing between the carbides along the Burgers vector direction and the spacing between neighboring slip planes from TEM observation, the total dislocation density required for the carbide coarsening is:

$$\rho = \frac{nL}{2L \times 150 \times 150}. \tag{13}$$

Equations (12) and (13) are plotted in Figure 6 using the typical experimental duration of a fatigue test. It is clear that the number of dislocation paths and the dislocation network density required to coarsen a carbide to an an average size of $L_{\text{Carbide}} \times W_{\text{Carbide}} \times H_{\text{Carbide}} = 16.5 \times 36.4 \times 100$ nm^3 within the experimental time decreases exponentially with increasing temperature. At 400 °C, a dislocation density of $\approx 1 \times 10^{16}\,\text{m}^{-2}$, which corresponds to more than 40 dislocation paths, is required to coarsen each carbide, which is unrealistically high for the current experiments. At 600 °C, only one dislocation path is required with a dislocation network density around the carbide on the order of $5 \times 10^{13}\,\text{m}^{-2}$. With further increase in temperature the required dislocation density to coarsen the carbides decreases even further. These results agree with the experimental observations that below 600 °C large carbide formation is highly unlikely. Above 1000 °C with the assumption made here for the relationship between bulk and pipe diffusion as disucssed for Eq. (11), pipe diffusion becomes less important or even irrelevant, and bulk diffusion likely dominates as the mechanism to transport all the required C atom to coarsen the carbides to the sizes observed in the experiments.

In the above analysis, the Cr lattice distortions due to C atoms was ignored, which can be refined in the future. Furthermore, the above analysis neglected the timescales associated with the diffusion of other elements (e.g. Cr, Ni etc.) and based on the assumption that the critical timescale is that for C transport. To check the validity of this assumption, the timescales for the diffusion of Cr and Ni atoms are investigated.

The number of Cr atoms required for the formation of carbide is:

$$N^f_{\text{Cr}} = \frac{V_{\text{carbide}}}{V_{\text{Cr}_{23}\text{C}_6}} \times 23 = 4.69 \times 10^6 \quad \text{atoms.} \tag{14}$$

The Cr bulk diffusion coefficient, D_{Cr}, in Nickel-base alloys containing Cr and Fe with C = 0.015 wt% is $1.6 \times 10^{-3} \times \exp(-36100/T)\text{m}^2\,\text{s}^{-1}$, while for those with C=0.070 w.% is $2.1 \times 10^{-2} \times \exp(-40900/T)\text{m}^2\,\text{s}^{-1}$, where T is in unit K [41]. Therefore, for the current analysis the Cr diffusion coefficient in René 88DT with C = 0.041 wt% at 650 °C is assumed to be the weighted average of the coefficients in those two alloys: $D_{\text{Cr}} \approx 9.4 \times 10^{-21}\,\text{m}^2\,\text{s}^{-1}$. Thus, the mean free path of Cr atoms (3D mean free path) at 650 °C is $L_{\text{Cr}} = (6D_{\text{Cr}}t)^{1/2} \approx 62$ nm.

The volume in the matrix having length $L_{\text{carbide}}+2L_{\text{Cr}}$, width $W_{\text{carbide}}+2L_{\text{Cr}}$, and height $H_{\text{carbide}}+2L_{\text{Cr}}$, contains $(L_{\text{carbide}}+2L_{\text{Cr}})\times(W_{\text{carbide}}+2L_{\text{Cr}})\times(H_{\text{carbide}}+2L_{\text{Cr}})/V_{\text{MatrixCell}}/1.66\times 84.5 = 7.1 \times 10^7$ Cr atoms, which is more than 15 times of N^f_{Cr}. Therefore, the experimental time associated with the fatigue experiment is sufficient for Cr diffusion to form the carbide.

Finally, assuming the Ni bulk diffusion coefficient in René 88DT is also on the same order of Cr, the mean free path of Ni atoms would be on the order of 60 nm, which indicates that the experimental time is also sufficient for Ni atoms to diffuse away from the carbide precipitate. Accordingly, within the experimental time, bulk diffusion of Cr and Ni atoms is sufficient for carbide formation such that their diffusion can be safely neglected as suggested.

5. Discussion

5.1. Deformation mode during cyclic loading

At intermediate and high temperatures, thermally activated processes play an important role in the cyclic deformation of superalloys by enhancing mechanisms such as cross slip [42, 43, 44]. With increasing temperature, the dislocation structures are observed to be more homogeneous [23, 45]. Nevertheless, planar slip with the evidence of γ' shearing still occurs at intermediate and high temperature during fatigue in the René 88DT [3]. From the investigation of the dislocation sub-structure of René 88DT specimens tested in fatigue at room temperature, 400°C and 650°C [3], individual slip bands with extensive shearing are observed early in the fatigue life near specific microstructure features. Also as temperature increases, the plastic localization is distributed over a greater number of parallel slip bands as shown in Figure 1(c-f) that develop near the specific twin boundaries in the parallel slip configuration [3], indicating a delocalization phenomenon with increasing temperature. This structure is forming a microscopic fatigue shear band that develops during cycling and leads to crack nucleation. The fatigue shear bands are very localized at room temperature (see Figure 1(a)), are formed from only a few parallel slip bands at 400°C, and have numerous parallel slip bands during fatigue at 650°C [3]. The fatigue localization is therefore more homogeneous and dispersed with increasing fatigue testing temperature, and as a consequence the surface crack density diminishes in the high cycle fatigue regime. During fatigue tests at 650°C, crack initiation is observed to shift to internal locations, while at room temperature initiation occurs at the surface [3].

Several mechanisms may explain the cyclic formation of multiple slip bands within the fatigue shear band. Hardening of the main gliding plane may prevent further dislocation motion on this plane and induce activation of other dislocation sources that glide on a plane parallel to the main gliding plane. Thermally activated processes such as cross slip may explain the formation of multiple slip bands within the fatigue shear band by double cross slip [24]. A combination of both hardening of main gliding plane and thermally activated processes may also be at the origin of the formation of multiple slip bands within the fatigue shear band. Three mechanisms may drive the hardening of the main gliding planes: (i) K-W locks, (ii) a strain aging effect that inhibits motion of mobile dislocations along the main glide planes and (iii) fine-scale precipitates that inhibit glide and force dislocations to cross slip out of the main glide plane.

It has been previously reported for nickel-base superalloys cycled at intermediate temperature that the mobile dislocations are impeded and the formation of additional dislocations or slip bands is required to accommodate the applied strain [42, 23, 46]. This phenomenon has been associated with the strain aging effect observed in several superalloys [17, 18, 19, 20]. Strain aging effects occur mainly due to low mobility solutes and the confined motion of dislocations along the {111} planes. The strain aging effect is generally evidenced by the serrated yielding (jerky flow, Portevin-Le Chatelier effect) that occurs during monotonic loading. Huron [18] has previously detailed serrated yielding in René 88DT at temperatures between 400°C and 593°C. Moreover, the strain rate sensitivity was negative valued for this temperature range. Huron [18] also indicated that the probable mechanism for the

serrated yielding was the interaction of carbon atoms with dislocations by dynamic strain aging. This was the first consideration that dislocations are affected by their surrounding carbon atmosphere. It is generally accepted that interstitial solutes are too mobile to exert a drag effect on moving dislocations at higher test temperatures and therefore, substitutional solutes must be responsible for the serrated flow behaviour and the impingement of dislocations [20, 21, 17, 22]. Of most interest, the serrated yielding does not occur at temperatures higher than 600°C [18], indicating that other effects are at the origin of the activation of multiple slip planes within the fatigue shear band at 650°C.

Precipitation of $Cr_{23}C_6$ is observed for the René 88DT at 650°C in Figure 3 while not observed at 400°C. Fine-scale carbide precipitation due to fatigue cycling was previously reported at intermediate temperatures along active slip bands and near boundaries for low carbon steel [47] and nickel-base superalloy [23, 19, 25]. The strong elastic interaction of carbon with dislocations favors carbon segregation and eventual carbide precipitation on dislocations. Precipitates that form at dislocations immobilize them, requiring the nucleation of new mobile dislocations to accommodate an imposed plastic strain [42]. Carbide precipitation depletes elemental carbon and chromium from interstitial positions, allowing dislocations to move more freely. Interestingly, carbide precipitation coincides with the end of the serrated yielding at temperatures above 650°C in René 88DT [18] and the end of the negative strain rate sensitivity associated with the strain aging effect.

The fine-scale precipitation along {111} slip planes within the fatigue shear band is certainly contributing to the hardening of the main gliding planes. Significant dislocation density is observed around the fine-scale carbides as shown in Figure 3(a). However, from the present research, it is not possible to conclude that this is the main mechanism bringing about the significant thickening of fatigue shear bands. Thermally activated processes such as cross-slip are likely to also play an important role in the thickening mechanism. While the formation of nano-scale carbide precipitation can be beneficial at 650°C, it is important to note that at higher temperature, the formation of larger carbides along slip bands may have a detrimental effect on fatigue life by embrittlement of the slip bands [23]. The developed model can inform us on the transition between the beneficial formation of a fine-scale of precipitates and the detrimental extended formation of carbides along the entirety of the slip bands.

5.2. Carbide nucleation and coarsening

A simplified diffusion model was used to describe the formation of fine-scale carbides. The nucleation and coarsening of carbides is controlled by the operating temperature. The carbide nucleation is assisted by supersaturation of C atoms driven by bulk diffusion, and the time required to reach supersaturation is strongly temperature dependent. At a lower temperature, it takes a very long time to reach supersaturation. While the time required for supersaturation is significantly shortened at higher temperatures. On the other hand, carbide coarsening is driven by C atom pipe diffusion along dislocations that are pinned at a carbide nucleus. Similar to the supersaturation, this process is also temperature-dependent. At a lower temperature, coarsening can hardly take place, but becomes more prevalent as temperatures increase. At a very high temperature, bulk diffusion dominates for atom

transportation and carbide coarsening. The analysis of the diffusion models shown here are in good agreement with the experimental observations by electron microscopy.

With minor modifications, this model can be applied to other alloys to study the formation of carbides. The diffusion model predicts the formation of carbides from a kinetic perspective. Even if the formation of carbides is possible through atom diffusion, thermodynamics should be accounted for to obtain the stable shape and size. The depletion of Cr from the matrix surrounding the carbides results in the formation of a layer of γ' at the carbide interface [48]. This interfacial energy results in a barrier for the growth of carbides.

The interaction between other elements and carbides is also important. In René 88DT, TiC and NbC carbides can react with Cr from the matrix to from $M_{23}C_6$, M_6C and M_7C_3 carbides. Despite the low concentrations of Ti and Nb, those types of carbides can have an unignorable impact on crack initiation during fatigue as well as damage resistance during high-temperature creep [49]. Using the details about those types of carbides, the presented diffusion model can be used to study the formation of other types of carbides and account for the carbide reactions.

Lastly, some simplifications made in the diffusion model can be improved to better predict the formation of carbides in alloys. One is utilizing more realistic diffusion coefficients, which are currently lacking in literature. Molecular dynamics simulations could be performed to obtain the diffusion data applicable for nickel-base superalloys. Another aspect is utilizing a constant value of the stress gradient $\nabla_{\boldsymbol{\xi}} P$. Stress gradients due to dislocations are usually on the orders of $\mathrm{MPa\,\mu m^{-1}}$, which in the same order as the value used in the current analysis. Nevertheless, the stress gradient can have strong local variations and can be orders of magnitudes higher. Under such circumstance, the simple inversely proportional relation of Eq. (12) does not hold anymore. A sophisticated numerical scheme is needed to correctly estimate the dislocation paths required for carbide coarsening.

6. Conclusion

The fatigue behavior of a polycrystalline nickel-base superalloy, René 88DT, was investigated during cycling loading in the high cycle fatigue regimes at 400°C and 650°C. Twin boundaries in the parallel slip configuration, where an active slip system is parallel to a twin plane, are the location of cyclic slip localization. Microscopic fatigue shear bands form during cycling. At intermediate and high temperature fatigue these shear bands thicken during cycling by activation of an increasing number of parallel slip planes. Fine-scale chromium carbide precipitation is observed along these {111} slip planes that are nearby twin boundaries in the parallel slip configuration. The formation of fine-scale carbides is observed to be controlled by diffusion rates of the superalloy chemical constituents. The carbide nucleation is found to be assisted by bulk diffusion, while the carbide coarsening is usually driven by pipe diffusion. The proposed model indicates that the the formation and size of the fine-scale carbide is strongly dependent on the temperature and duration of the fatigue experiment.

7. Acknowledgments

The authors gratefully acknowledge the support of GE Global Research, AFOSR/AFRL for sponsoring Center of Excellence on Integrated Materials Modeling (CEIMM – Grant FA9550-12-1-0445) and the Air Force Center of Excellence (Grant FA9550-12-1-0445) and US Department of Energy Basic Energy Sciences Grant DE-SC0018901. The authors also appreciate useful discussions with J. Laflen and A. Loghin.

References

[1] R. C. Reed, The Superalloys, Cambridge University Press, 2006, cambridge Books Online.

[2] D. Texier, J. Cormier, P. Villechaise, J.-C. Stinville, C. J. Torbet, S. Pierret, T. M. Pollock, Crack initiation sensitivity of wrought direct aged alloy 718 in the very high cycle fatigue regime: the role of non-metallic inclusions, Materials Science and Engineering: A 678 (2016) 122 – 136. doi:http://dx.doi.org/10.1016/j.msea.2016.09.098.

[3] J. C. Stinville, E. Martin, M. Karadge, S. Ismonov, M. Soare, T. Hanlon, S. Sundaram, M. P. Echlin, P. G. Callahan, W. C. Lenthe, V. Miller, J. Miao, A. E. Wessman, R. Finlay, A. Loghin, J. Marte, T. M. Pollock, Fatigue deformation in a polycrystalline nickel base superalloy at intermediate and high temperature: Competing failure modes, Acta Materialia 152 (2018) 16 – 33. doi:https://doi.org/10.1016/j.actamat.2018.03.035.

[4] J. Miao, T. M. Pollock, J. Wayne Jones, Crystallographic fatigue crack initiation in nickel-based superalloy René 88DT at elevated temperature, Acta Materialia 57 (20) (2009) 5964–5974. doi:10.1016/j.actamat.2009.08.022.

[5] J. Miao, T. M. Pollock, J. Wayne Jones, Microstructural extremes and the transition from fatigue crack initiation to small crack growth in a polycrystalline nickel-base superalloy, Acta Materialia 60 (6–7) (2012) 2840 – 2854. doi:http://dx.doi.org/10.1016/j.actamat.2012.01.049.

[6] J. C. Stinville, W. C. Lenthe, J. Miao, T. M. Pollock, A combined grain scale elastic-plastic criterion for identification of fatigue crack initiation sites in a twin containing polycrystalline nickel-base superalloy, Acta Materialia 103 (2015) 461–473. doi:10.1016/j.actamat.2015.09.050.

[7] S. T. Wlodek, M. Kelly, D. A. Alden, The structure of René 88DT, Superalloys 1996 (1996) 129–136.

[8] C. A. Stein, A. Cerrone, T. Ozturk, S. Lee, P. Kenesei, H. Tucker, R. Pokharel, J. Lind, C. Hefferan, R. M. Suter, A. R. Ingraffea, A. D. Rollett, Fatigue crack initiation, slip localization and twin boundaries in a nickel-based superalloy, Current Opinion in Solid State and Materials Science 18 (4) (2014) 244 – 252, slip Localization and Transfer in Deformation and Fatigue of Polycrystals. doi:http://dx.doi.org/10.1016/j.cossms.2014.06.001.

[9] J. C. Stinville, P. G. Callahan, M. A. Charpagne, M. P. Echlin, V. Valle, T. M. Pollock, Direct measurements of slip irreversibility in a nickel-based superalloy using high resolution digital image correlation, Acta Materialia 186 (2020) 172 – 189. doi:https://doi.org/10.1016/j.actamat.2019.12.009.

[10] J. C. Stinville, W. C. Lenthe, M. P. Echlin, P. G. Callahan, D. Texier, T. M. Pollock, Microstructural statistics for fatigue crack initiation in polycrystalline nickel-base superalloys, International Journal of Fracture 208 (2017) 221 – 240. doi:https://doi.org/10.1007/s10704-017-0241-z.

[11] D. Khireddine, M. H. Khireddine, Low cycle fatigue behaviour of an aluminium alloy with small shearable precipitates: Effect of surface coating, International Journal of Fatigue 22 (7) (2000) 585 –

591. doi:http://doi.org/10.1016/S0142-1123(00)00028-1.

[12] Y. Brechet, F. Louchet, On the stability of orowan loops around coherent spherical ordered precipitates, Acta Metallurgica 37 (9) (1989) 2469 – 2473. doi:http://dx.doi.org/10.1016/0001-6160(89)90044-8.

[13] H. S. Ho, M. Risbet, X. Feaugas, On the unified view of the contribution of plastic strain to cyclic crack initiation: Impact of the progressive transformation of shear bands to persistent slip bands, Acta Materialia 85 (2015) 155 – 167. doi:http://doi.org/10.1016/j.actamat.2014.11.020.

[14] H. Mughrabi, Specific features and mechanisms of fatigue in the ultrahigh-cycle regime, International Journal of Fatigue 28 (2006) 501–508.

[15] J. C. Stinville, N. Vanderesse, F. Bridier, P. Bocher, T. M. Pollock, High resolution mapping of strain localization near twin boundaries in a nickel-based superalloy, Acta Materialia 98 (2015) 29–42. doi:10.1016/j.actamat.2015.07.016.

[16] B. H. Kear, H. G. F. Wilsdorf, Dislocation configurations in plastically deformed polycrystalline Cu_3Au alloys, Transactions of the Metallurgical Society of AIME 224 (1962) 382.

[17] R. A. Mulford, K. U. F., New observations on the mechanisms of dynamic strain aging and of jerky flow, Acta Metallurgica 27 (1979) 1125–1134.

[18] E. Huron, Serrated yielding in a nickel-base superalloy, Superalloys 1992 (1992) 675–684.

[19] B. A. Lerch, G. V., The low cycle fatigue properties of a $\gamma\prime$ strengthened superalloy, in Bilde-Sorensen J B, Hansen N, Horsewell A, Leffers T, Lilholt H, editors. Deformation of multi-phase and particle containing material: proceedings of the 4th Riso international symposium on metallurgy and materials science, Roskilde, Denmark: Riso National Laboratory (1983) 375–380.

[20] A. K. Koul, F. B. Pickering, Serrated yielding in Ni-Fe base superalloys at 700°C, Scripta Metallurgica 16 (1982) 119–124.

[21] G. Carotenuto, A. DeIorio, A. Gallo, C. Luvidi, The serrated flow in a nickel-base superalloy, Engineering Materials Advisory Services (1995) 89–101.

[22] A. W. Sleeswyk, Slow strain-hardening of ingot iron, Acta Metallurgica 6 (1958) 598–603.

[23] B. A. Lerch, N. Jayaraman, S. D. Antolovich, A study of fatigue damage mechanisms in Waspalloy from 25 to 800°C, Materials Science and Engineering 66 (1984) 151–166.

[24] A. M. Hussein, S. I. Rao, M. D. Uchic, D. M. Dimiduk, J. A. El-Awady, Microstructurally based cross-slip mechanisms and their effects on dislocation microstructure evolution in fcc crystals, Acta Materialia 85 (Supplement C) (2015) 180 – 190. doi:https://doi.org/10.1016/j.actamat.2014.10.067.

[25] A. Cervellon, S. Hémery, P. Kürnsteiner, B. Gault, P. Kontis, J. Cormier, Crack initiation mechanisms during very high cycle fatigue of Ni-based single crystal superalloys at high temperature, Acta Materialia 188 (2020) 131 – 144. doi:https://doi.org/10.1016/j.actamat.2020.02.012.

[26] D. D. Krueger, R. D. Kissinger, R. G. Menzies, Developement and introduction of a damage tolerant high temperature nickel-base disk alloy, René 88DT, Superalloy 1992 (1992) 277.

[27] M. J. Caton, S. K. Jha, A. H. Rosenberger, A. H. Larsen, Divergence of mechanisns and the effect on the fatigue life variability of the René 88DT, Superalloy 2004 (2004) 305–312.

[28] T. F. Lui, S. W. Peng, Y. L. Lin, C. C. Wu, Orientation relationships among M23C6, M6C, and austenite in an Fe-Mn-Al-Mo-C alloy, Metallurgical transactions A 21 (1990) 567–574.

[29] W. Kesternich, Dislocation-controlled precipitation of TiC particles and their resistance to coarsening, Philosophical Magazine A 52 (4) (1985) 533–548. doi:10.1080/01418618508237645.

[30] K. Persson, Materials data on $Cr_{23}C_6$ (SG:225) by Materials Project, an optional note (April 2016). doi:10.17188/1287577.

[31] H. Mehrer, Diffusion in solids: fundamentals, methods, materials, diffusion-controlled processes, Vol. 155, Springer Science & Business Media, 2007.
[32] G. E. Murch, Diffusion in crystalline solids, Academic Press, 2012.
[33] I. Matsui, T. Uesugi, Y. Takigawa, K. Higashi, Effect of interstitial carbon on the mechanical properties of electrodeposited bulk nanocrystalline Ni, Acta Materialia 61 (9) (2013) 3360 – 3369. doi:https://doi.org/10.1016/j.actamat.2013.02.025.

[34] J. J. Lander, H. E. Kern, A. L. Beach, Solubility and diffusion coefficient of carbon in nickel: Reaction rates of nickel-carbon alloys with barium oxide, Journal of Applied Physics 23 (12) (1952) 1305–1309. doi:10.1063/1.1702064.

[35] C. Krempaszky, U. Liedl, E. A. Werner, A note on the diffusion of carbon atoms to dislocations, Computational Materials Science 38 (1) (2006) 90 – 97. doi:https://doi.org/10.1016/j.commatsci.2006.01.010.

[36] J. Y. Hwang, R. Banerjee, J. Tiley, R. Srinivasan, G. B. Viswanathan, H. L. Fraser, Nanoscale characterization of elemental partitioning between gamma and gamma prime phases in René 88 DT nickel-base superalloy, Metallurgical Transactions A 40 (40) (2009) 24–35. doi:https://doi.org/10.1007/s11661-008-9691-2.
[37] M. Legros, G. Dehm, E. Arzt, T. J. Balk, Observation of giant diffusivity along dislocation cores, Science 319 (5870) (2008) 1646–1649. arXiv:http://science.sciencemag.org/content/319/5870/1646.full.pdf, doi:10.1126/science.1151771.

[38] P. M. Anderson, J. P. Hirth, J. Lothe, Theory of dislocations, Cambridge University Press, 2017.
[39] R. Li, Q. Xie, Y. Wang, W. Liu, M. Wang, G. Wu, X. Li, M. Zhang, Z. Lu, C. Ge, T. Zhu, Unraveling submicron-scale mechanical heterogeneity by three-dimensional x-ray microdiffraction, Proceedings of the National Academy of Sciences 115 (3) (2018) 483–488.
[40] A. Ishii, J. Li, S. Ogata, "Conjugate channeling" effect in dislocation core diffusion: Carbon transport in dislocated BCC iron, PLoS ONE 8 (4) (2013) e60586. doi:10.1371/journal.pone.0060586.

[41] T.-F. Chen, G. Tiwari, Y. Iijima, K. Yamauchi, Volume and grain boundary diffusion of chromium in Ni-base Ni-Cr-Fe alloys, Mater. Trans. 44 (1) (2003) 40–46. doi:10.2320/matertrans.44.40.
[42] A. Pineau, S. D. Antolovich, High temperature fatigue of nickel-base superalloys – A review with special emphasis on deformation modes and oxidation, Engineering Failure Analysis 16 (8) (2009) 2668–2697. doi:10.1016/j.engfailanal.2009.01.010.

[43] W. W. Milligan, S. D. Antolovich, Yielding and deformation behavior of the single crystal superalloy PWA 1480, Metallurgical Transactions A 18 (1) (1987) 85–95. doi:10.1007/BF02646225.

[44] G. B. Viswanathan, P. Sarosi, M. Henry, D. Whitis, M. Mills, Deformation mechanisms at intermediate creep temperatures in René 88DT, Superalloys 2004, Edited by K.A. Green, T.M. Pollock, H. Harada, T.E. Howson, R.C. Reed, J.J. Schirra, and S, Walston, TMS (The Minerals, Metals & Materials Society), 2004 (2004) 173–178.
[45] B. A. Lerch, Microstructural effects on the room and elevated temperature low cycle fatigue behavior of Waspaloy, NASA CR-165497 (1982).
[46] C. H. Wells, C. P. Sullivan, the effect of temperature on the low cycle fatigue behavior of UDIMET 700, Trans. ASM 60 (1967) 217–222.
[47] D. V. Wilson, Precipitation and growth of carbide particles in a cyclically strained low-carbon steel, Acta Metallurgica 21 (1973) 673–682.
[48] T. M. Pollock, S. Tin, Nickel-based superalloys for advanced turbine engines: chemistry, microstructure and properties, Journal of Propulsion and Power 22 (2) (2006) 361–374.

[49] F. I. Versnyder, M. E. Shank, The development of columnar grain and single crystal high temperature materials through directional solidification, Materials Science and Engineering 6 (4) (1970) 213–247.

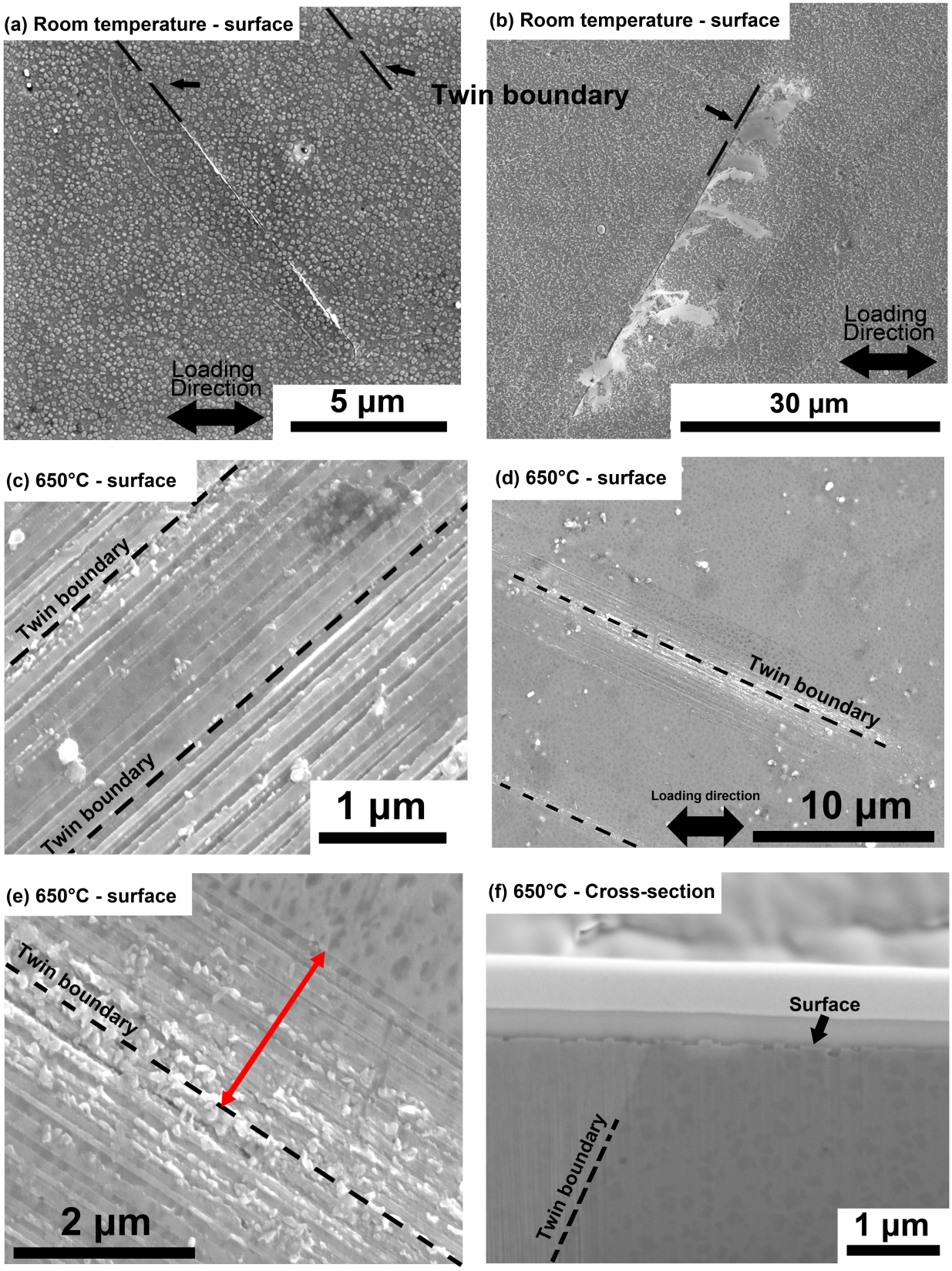

Figure 1: Plastic localization occurring during cyclic loading for specimen tested at room temperature (a-b) and at 650°C (c-f) in the high cycle fatigue regime. (b) Adapted from [6]. The fatigue tests were interrupted at 45% (a-b) and 80% (c-f) of fatigue life. (a-e) Occurrence of a microscopic fatigue shear bands near twin boundaries at the specimen surface. (f) FIB cross-section from a location near a twin boundary displaying surface extrusion. The cross-section was performed perpendicular to the twin boundary.

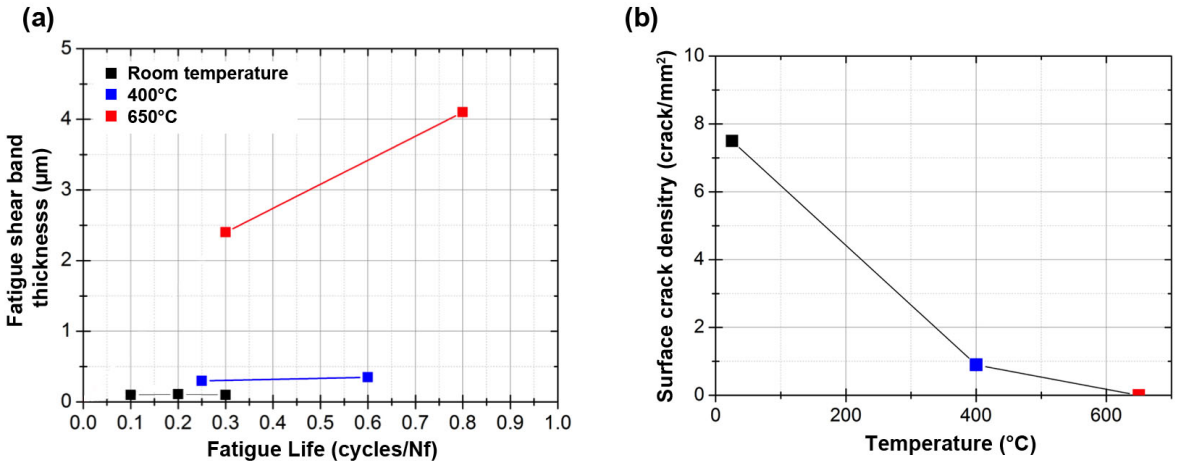

Figure 2: (a) Average thickness of fatigue shear bands at the surface of the specimen as a function of the normalized fatigue life for specimens tested at room temperature, 400°C and 650°C. The thickness of a fatigue shear band is defined as the distance between the twin boundary and the farthest slip trace that constitutes the fatigue shear band as depicted by the red arrow in Figure 1(e). (b) Surface crack density at 80% of fatigue life for specimen tested at room temperature, 400°C and 650°C.

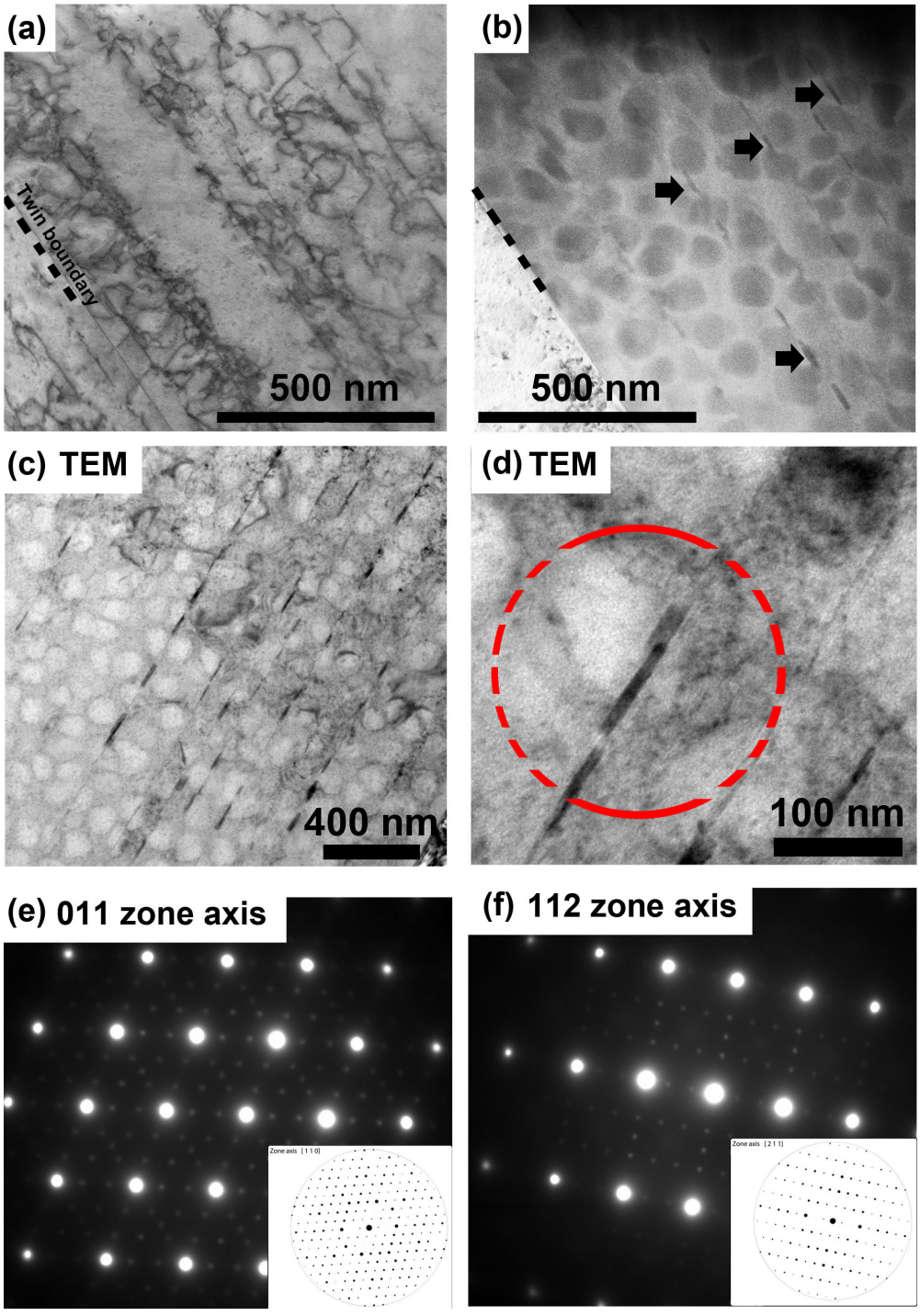

Figure 3: Fine scale precipitation during fatigue cycling for a specimen tested at 650°C: (a) High angle annular dark field STEM images from a location near a twin boundary displaying a high density of dislocations. The TEM foil was extracted perpendicular to a twin boundary displaying a microscopic fatigue shear band. The contrast of the image has been inverted for better visual of the dislocation. (b) The associated STEM image in phase contrast showing shearing of γ' and fine scale precipitation in the γ matrix. (c) The associated conventional TEM image. Image are flipped with regard to (a) and (b). (d) High magnification TEM images of the precipitation along slip bands that form during fatigue. (e and f) Diffraction pattern from the volume displayed by the red circle in (d). The diffraction patterns correspond to the combination of the Ni_3Al phase and $M_{23}C_6$ carbide.

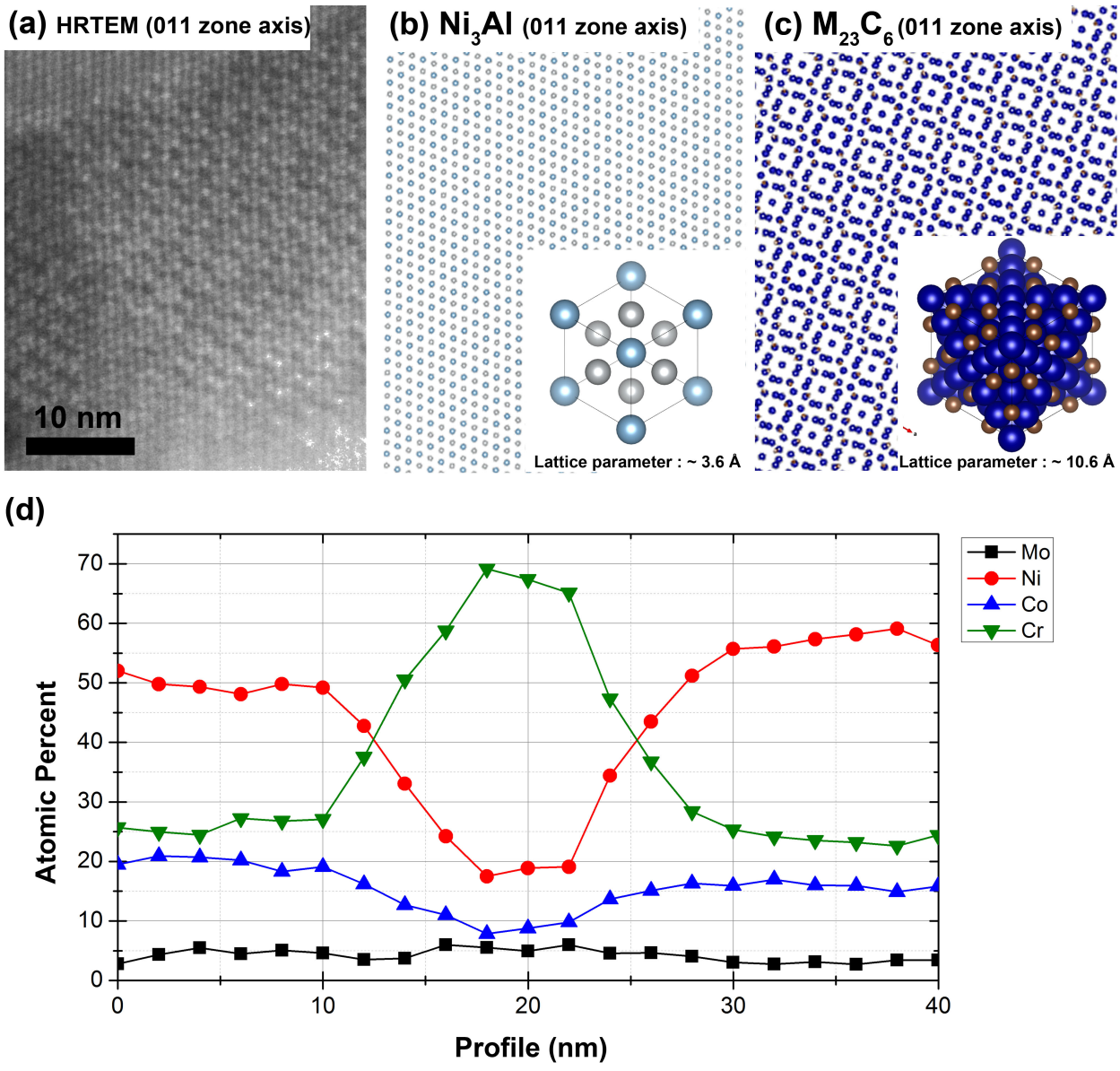

Figure 4: (a) High resolution TEM imaging of the precipitation induced during fatigue cycling at 650°C. (b-c) Simulated stress-free atomistic arrangement for the Ni_3Al and $M_{23}C_6$ phases. (d) Chemical composition extracted from HRTEM energy dispersive X-ray along a line scan across the precipitated phase.

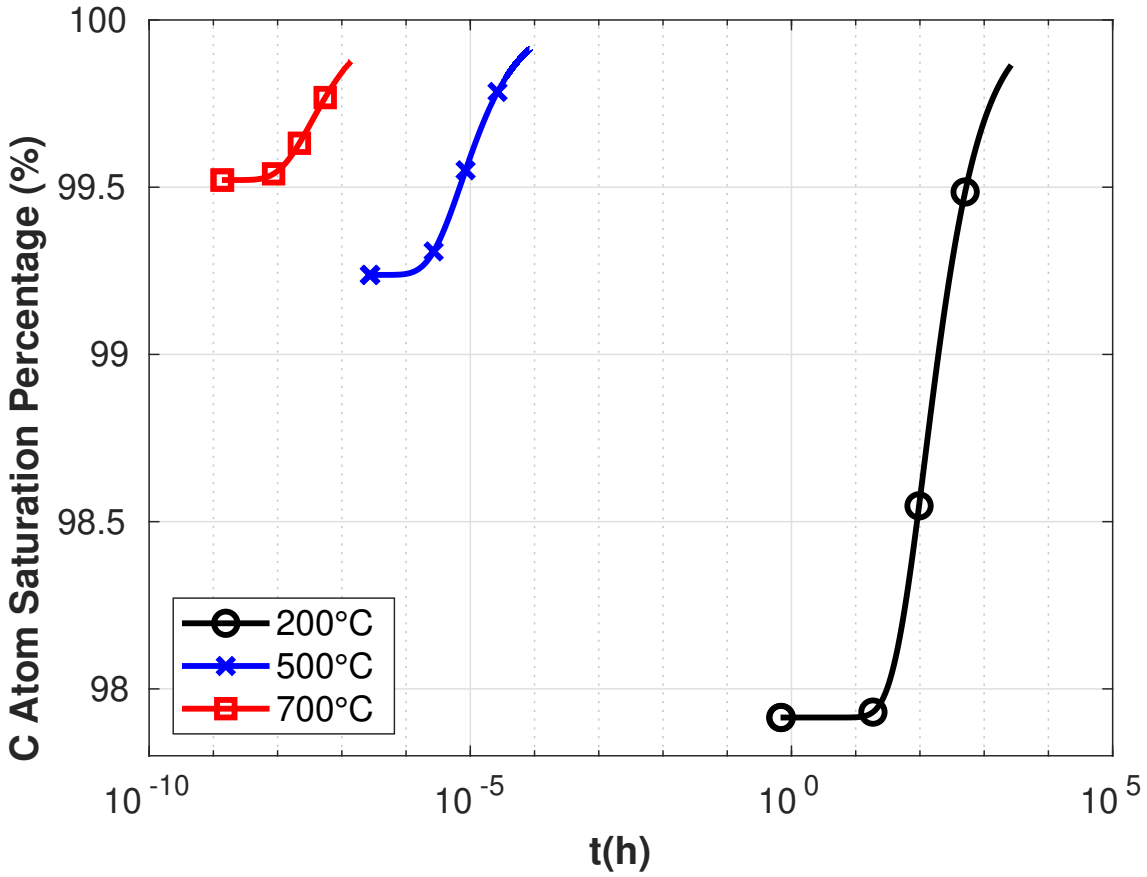

Figure 5: The C atom saturation percentage around an edge dislocation as a function of time for three different temperatures: 200 °C, 500 °C and 700 °C.

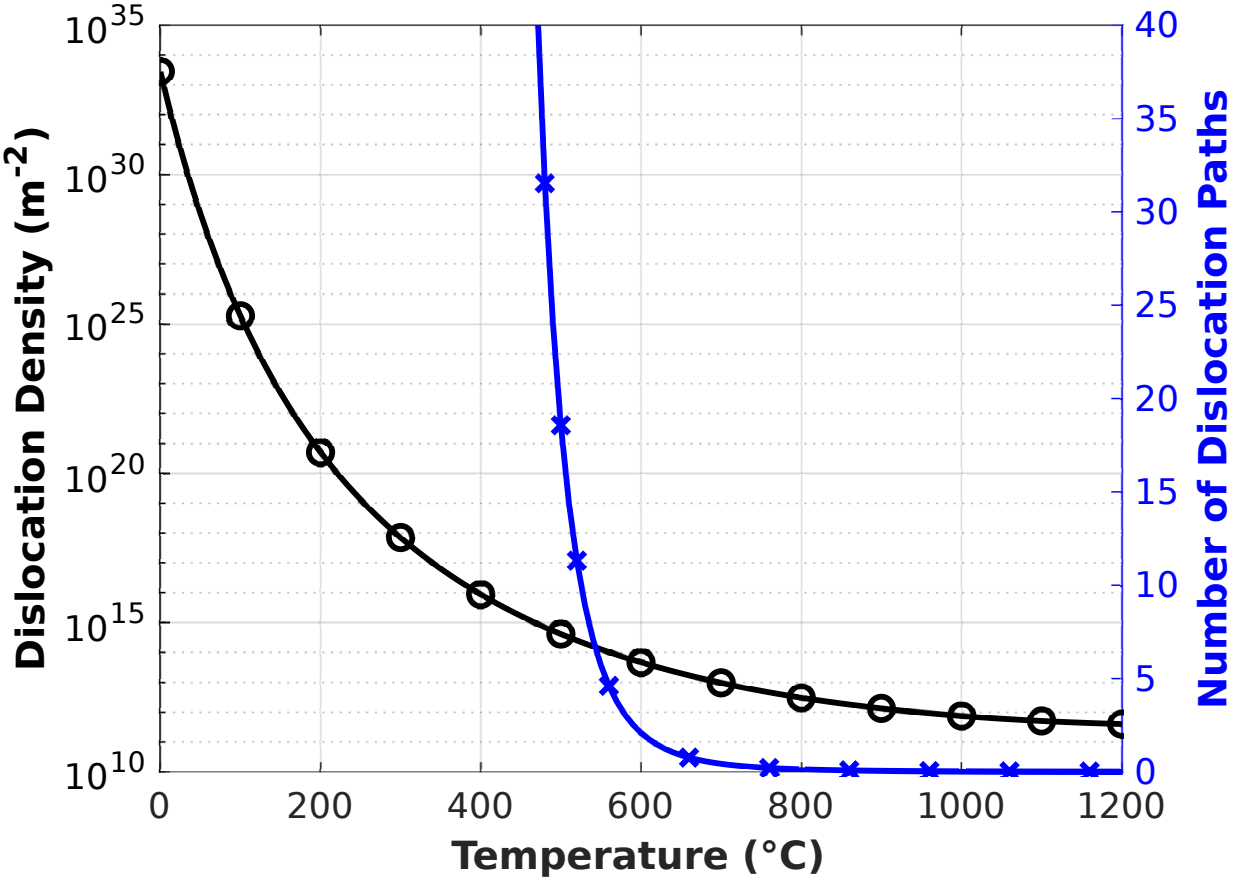

Figure 6: The local dislocation density (black) around the carbide and the number of dislocation paths (blue) connected to the carbide required to coarsen the carbides to a size 16.5 × 36.4 × 100 nm^3 within 19 hours.